Terrain-flattened gamma nought Radarsat-2 backscatter

Small, David ; Zuberbühler, Lukas ; Schubert, Adrian ; Meier, Erich

Abstract: Radarsat-2 offers a variety of new modes and capabilities. We present results from rigorous application of geometric and radiometric calibration to backscatter values, enabling comparisons between different modes. First, the system's a priori geometric accuracy was tested (tiepoint free) by comparing the measured positions of corner reflectors in ultrafine images with predicted locations calculated based on the satellite state vectors and radar timing annotations. Second, the geometric accuracy of the dual-pol ScanSAR SCNB mode was tested by correlating each backscatter image to a radar image simulation calculated using the same product annotations. Third, the radar image simulation was used to normalize the backscatter values in both polarisations, generating terrain-flattened gamma nought values that were then terrain geocoded. Fourth, the available ascending and descending SCNB image pair was overlaid with and without such radiometric terrain correction applied. The advantages gained by using terrain-flattened gamma nought are discussed.

DOI: https://doi.org/10.5589/m11-059

Can. J. Remote Sensing, Vol. 37, No. 5, pp. 493–499, 2011

Research Note / Note de recherche

Terrain-flattened gamma nought Radarsat-2 backscatter

David Small, Lukas Zuberbühler, Adrian Schubert, and Erich Meier

Abstract. Radarsat-2 offers a variety of new modes and capabilities. We present results from rigorous application of geometric and radiometric calibration to backscatter values, enabling comparisons between different modes. First, the system's a priori geometric accuracy was tested (tiepoint free) by comparing the measured positions of corner reflectors in ultrafine images with predicted locations calculated based on the satellite state vectors and radar timing annotations. Second, the geometric accuracy of the dual-pol ScanSAR SCNB mode was tested by correlating each backscatter image to a radar image simulation calculated using the same product annotations. Third, the radar image simulation was used to normalize the backscatter values in both polarisations, generating terrain-flattened gamma nought values that were then terrain geocoded. Fourth, the available ascending and descending SCNB image pair was overlaid with and without such radiometric terrain correction applied. The advantages gained by using terrain-flattened gamma nought are discussed.

Résumé. RADARSAT-2 offre une variété de nouveaux modes et fonctionnalités. Nous présentons les résultats obtenus par l'application rigoureuse de la calibration géométrique et radiométrique sur les valeurs de rétrodiffusion, permettant de comparer les différents modes. Premièrement, la précision géométrique a priori du système est testée (sans points de soutien) en comparant les positions de réflecteurs trièdres mesurées sur les images ultra-fines avec les positions prévues, ces dernières étant calculées à partir des annotations contenant les vecteurs d'état du satellite ainsi que les paramètres temporaux du radar. Deuxièmement, la précision géométrique du mode ScanSAR en polarisation double (appelé SNCB) est testée en corrélant chaque image de rétrodiffusion avec une image radar simulée, générée en utilisant les vecteurs d'état et les paramètres temporaux extraits des annotations en combinaison avec un MNT. Troisièmement, cette image radar simulée est utilisée pour normaliser les valeurs de rétrodiffusion des deux polarisations, générant des valeurs de gamma zéro normalisées selon le relief, qui sont ensuite géocodées. Quatrièmement, la paire d'images SCNB (1 × ascendante, 1 × descendante) est superposée une fois sans et une fois avec l'application de cette correction radiométrique du terrain. Les avantages de l'utilisation de gamma zéro normalisé selon le relief sont discutés.
[Traduit par la Rédaction]

Introduction

Both the geometric and radiometric quality of any synthetic aperature radar (SAR) sensor determines whether or not its data can be applied to the wide range of SAR applications. Maximizing the accuracy of tiepoint-free geolocation ensures that SAR products can be easily combined with other geospatial data. This enables a combination of SAR imagery and its derivative products with digital elevation models (DEMs) (Meier et al., 1993). The same DEMs may also be used to terrain flatten the retrieved backscatter values (Small, 2011).

The beta nought (β^0) backscatter convention (Raney et al., 1994) is best used when storing level 1 radar backscatter values in slant range geometry, as it offers the least encumbered methodology for keeping the actual radar measurements. Translation of the recorded backscatter values into the sigma nought (σ^0) or gamma nought (γ^0) conventions requires the use of an Earth model, either a simple ellipsoidal Earth (Rosich and Meadows, 2004; ESA, 2007), or a more detailed DEM. In the former case, the subscript E can be used to indicate the use of an Ellipsoidal Earth model (σ^0_E and γ^0_E), while in the latter case, the subscript T can be used (σ^0_T and γ^0_T) to indicate the use of a terrain model (Small et al., 2009a). The radiometric look-up tables (LUTs) included with Radarsat-2 (R2) products (MDA, 2008) were generated using an ellipsoidal Earth model. When an image simulation is performed conforming

Received 31 March 2011. Accepted 14 September 2011. Published on the Web at http://pubs.casi.ca/journal/cjrs on 8 March 2012.

D. Small[1], L. Zuberbühler, A. Schubert, and E. Meier. Remote Sensing Laboratories, Dept. of Geography, University of Zurich, Winterthurerstrasse 190, CH-8057 Zurich, Switzerland.

[1]Corresponding author (e-mail: david.small@geo.uzh.ch).

strictly to the gamma nought convention while integrating all available height information, including checks for local occlusions (radar shadow), then the actual area visible to the radar (in the plane perpendicular to the slant range plane) can be retrieved. A method to estimate that area and then also the backscatter parameter known as terrain-flattened gamma nought (γ^0_T) was described in Small (2011).

Tiepoint-free geolocation accuracy

A pair of ascending and descending ultrafine (UF) R2 images was acquired from Torny-le-Grand, Switzerland on 2 March and 10 May 2010. Two pairs of corner reflectors (CRs) were deployed within each scene; their phase centres were surveyed using a differential global positioning system (DGPS) (Small et al., 2004; Schubert et al., 2010). The surveyed coordinates were used in combination with the satellite's state vectors and radar timing annotations provided in the SAR product header to predict the location of each coordinate within each image raster. That prediction was then compared with the actual measured image location calculated to subsample accuracy by virtue of oversampling. Close-ups of the corner reflectors in each image are shown in **Figure 1**.

The predictions are shown with yellow crosses at full single-look complex (SLC) resolution. The actual measured corner reflector locations are visible in the images themselves. As the two CRs were quite close to each other, there was some overlap in the regions surrounding each prediction cross. Although the range prediction's accuracy was less than 1 UF SLC sample, an azimuth bias of 10–12 UF SLC samples was detected. When the same geolocation methodology is applied to products from the instruments ASAR (ESA ENVISAT), PALSAR (JAXA ALOS), or TSX (DLR/InfoTerra TerraSAR-X), no such azimuth bias is detectable. In the case of ASAR products processed with the standard ESA ASAR processing facility (PF-ASAR), a deterministic "azimuth bistatic shift" must be compensated (Small et al., 2004) but that induces no requirement for the use of tiepoints to achieve accuracy within two SLC samples. That accuracy level was not achieved with the R2 data. It would be premature to make a system-wide statement on R2 geolocation accuracy based on only two images that include CRs, so the results are reported only as evaluated. Further tests with a diverse set of imagery would be required before one would be able to make a credible statement with broader applicability.

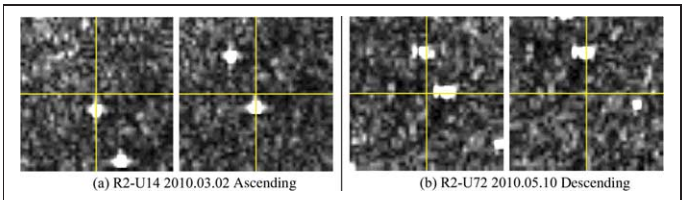

Figure 1. R2 Ultra-fine geolocation tests using corner reflectors, (a) U14 ascending 2 March 2010 and (b) U72 descending 10 April 2010.

ScanSAR Azimuth timing offset

Tests of geolocation accuracy were also performed on a single pair of ascending and descending R2 ScanSAR Narrow B (SCNB) images acquired over Switzerland in April 2010. The SCNB products tested were dual-pol VH/VV images with 50 m resolution acquired within 12 hours of each other. No corner reflectors were deployed for these acquisitions. The geometry of these wide-swath products was instead tested by comparing the backscatter image with a DEM-based image simulation calculated in the Alpine region, where strong contrast was available between regions subject to foreshortening and layover on foreslopes and occlusions and (or) radar shadow on backslopes. The image simulation was generated using the Swiss DHM25 height model (25 m resolution) as input (swisstopo, 2005). The correlation and geometry-refinement operation (Small et al., 2000) was performed using SCNB products acquired on 26 April 2010 17:23:36 coordinated universal time (UTC) (ascending), and 27 April 2010 05:33:21 UTC (descending). For the ascending case, simulated versus measured backscatter are shown in **Figure 2a** and **2b**, respectively. In both of the products available, an azimuth offset of slightly more than 0.2 s was estimated between the simulation and measurement. The red arrows indicate the azimuth dimension of the shift. The 0.2 s increment was very close to the azimuth time increment between the azimuth time at the beginning of each image raster and the first line not filled by null cell values, much larger than the small offsets observed in the UF images that was discussed in the previous section. The null cell values at the "first azimuth" edges are illustrated in **Figure 3**.

The azimuth start time was assigned to the first non-null cell value line rather than the beginning of the raster (the timing definition listed in the product format documentation). No other adjustments were made to the state vector or radar timing annotation information. Given the above simple adjustment, good correspondence was found

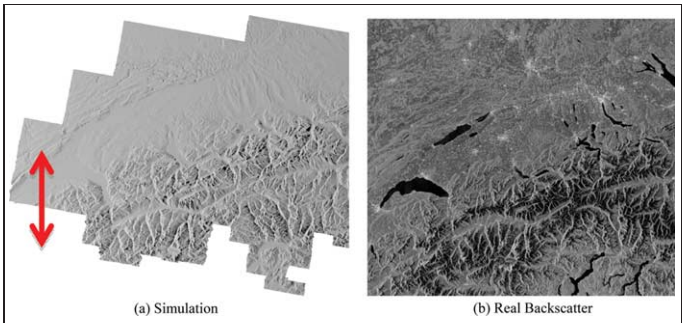

Figure 2. Radarsat-2 SCNB 26 April 2010 ascending ground range images, (a) image simulation, (b) γ^0_E VV backscatter measurement (black, −20 dB; white, 5 dB).

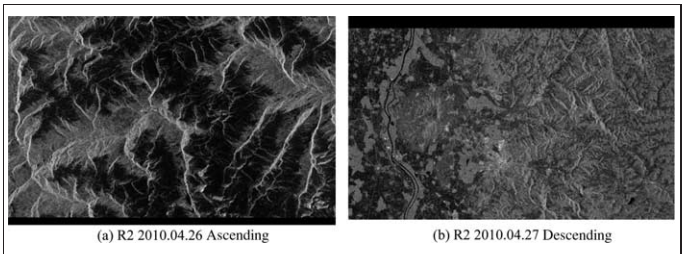

Figure 3. Azimuth image edges, Radarsat-2 SCNB azimuth timing annotation offset. Extracts at early azimuth (VH).

between the simulations and real measurements. In all further processing, the adjusted azimuth time was used.

Terrain-flattened gamma nought

Given the highly accurate knowledge of a SAR sensor's geometry, it becomes possible to treat its radiometry (backscatter) in a more robust manner by including an Earth model that incorporates a DEM within the backscatter retrieval process. Radiometric terrain correction (RTC) contrasts with standard terrain geocoding procedures, whereby σ^0_E or γ^0_E backscatter values estimated originally in radar geometry (slant or ground range) are resampled one-to-one onto a DEM grid. Although the position, or geometry, of backscatter estimates are corrected in Geometrically-Terrain-Corrected (GTC) products, the radiometry of resulting GTC imagery never severs its ties to the ellipsoid model that was used during the original backscatter estimation.

Backscatter estimates made using an ellipsoidal Earth model were contrasted with those performed incorporating a DEM. For the ellipsoid case, the standard product gamma nought LUT was consulted (MDA, 2008). In the case of terrain-flattened gamma nought, the methodology described within Small et al. (2010) and Small (2011) was employed. The method uses a terrain model to calculate local normalization areas individually via image simulation for each range and azimuth sample in radar geometry. That reference area is then used during retrieval of the backscatter coefficient (backscatter per unit area). The image simulation methodology was pioneered by Guindon and Adair (1992) and extended in Small (2011) with steps that include (*i*) occlusion checks, (*ii*) addition of a method to distribute areas more accurately in radar geometry, and (*iii*) strict adherence to the gamma nought convention for the normalization area.

The R2 SCNB ascending product acquired over Switzerland on 26 April 2010 is illustrated in its native ground range geometry in **Figure 4.** The VH polarization is shown in **Figure 4a** and the VV in **Figure 4b**). The radiometric scaling extends from −26 dB (black) to −1 dB (white) for VH, and −20 dB (black) to 5 dB (white) for VV. The dynamic range is 25 dB in all cases. Conventional terrain-geocoded versions of the γ^0_E backscatter values are shown in **Figure 4c**, γ^0_E VH, and **Figure 4d**, γ^0_E VV. The jagged image edges indicate the limits of the DHM25 height model (swisstopo, 2005). Radiometric terrain correction was applied during γ^0_T backscatter retrieval, resulting in the images shown in **Figure 4e**, γ^0_T VH, and **Figure 4f**, γ^0_T VV. A similar set of images for the R2 SCNB descending product acquired over Switzerland on 27 April 2010 is shown in **Figure 5**.

Ground range representations of γ^0_E (VH) and γ^0_E (VV) are shown in **Figures 5a** and **b**, respectively. Conventional terrain geocoded versions of the γ^0_E backscatter values are shown in **Figure 5c**, γ^0_E VH, and **Figure 5d**, γ^0_E VV. Radiometric terrain correction was applied during γ^0_T backscatter retrieval, resulting in the images shown in **Figure 5e**, γ^0_T VH, and **Figure 5f**, γ^0_T VV. Terrain-induced effects are confounded with thematic landcover induced backscatter in the GTC imagery. By contrast, in the RTC imagery the terrain effects were "flattened", and a less ambiguous estimate of landcover-induced backscatter values became possible. Dark wet snow was seen at intermediate elevations and dry bright snow at higher elevations (e.g., Jungfrau and Valais mountains) where snow melting had not yet started at the time the images were acquired in late April. The VH polarization appeared to be more sensitive to wet snow cover than VV. Experience to date indicates that the terrain flattening works best for cross-pol data (VH or HV), but it also works well on co-pol VV imagery, as seen in **Figures 4** and **5**. Greater residuals were observed after flattening HH data, possible improvements are being investigated.

Ascending and descending overlays

The VH γ^0_E backscatter estimates from the ascending and descending SCNB products were terrain geocoded onto the same Swiss map grid, and are overlaid in **Figure 6a**. The terrain-flattened gamma nought γ^0_T is overlaid in a similar manner in **Figure 6b**. Conventional wisdom holds that the backscatter mechanism varies strongly with the nominal incident angle as one proceeds from the near-range portion of the swath towards the far-range section. If that were always true, then one would see that trend here amplified by a factor of two, as the direction of the trend in the ascending case is opposite to the descending case. Yet inspection of **Figure 6b** reveals that no such trend is visible for the forest, bare field, water surface, or settlement land cover types. The backscatter mechanism is relatively stable within a useful range of nominal incident angles. Density plots in **Figures 6c–f** use the legend's colours to illustrate the local density (logarithmic colour distribution). Strong opposing trends between ascending and descending in γ^0_E backscatter are seen in **Figures 6a** and **c**, as bright foreslopes in one configuration become relatively dark backslopes in the other. The opposing trends (and bias) are calmed in **Figure 6d** after terrain flattening was applied. The opposing trends are visible in the local reference area

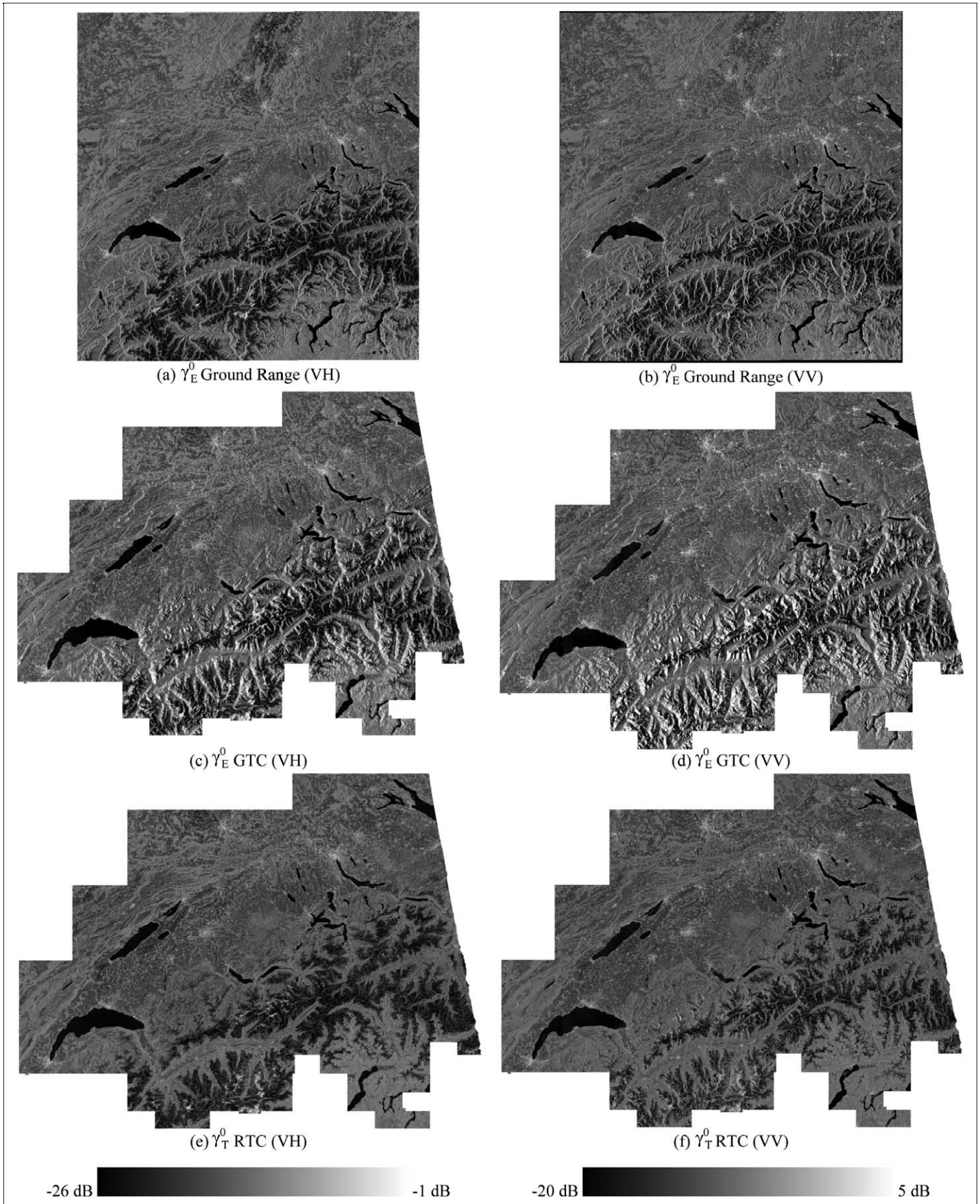

Figure 4. Radarsat-2 SCNB VH/VV, 26 April 2010, ascending. DHM25 used for terrain geocoding and radiometric corrections.

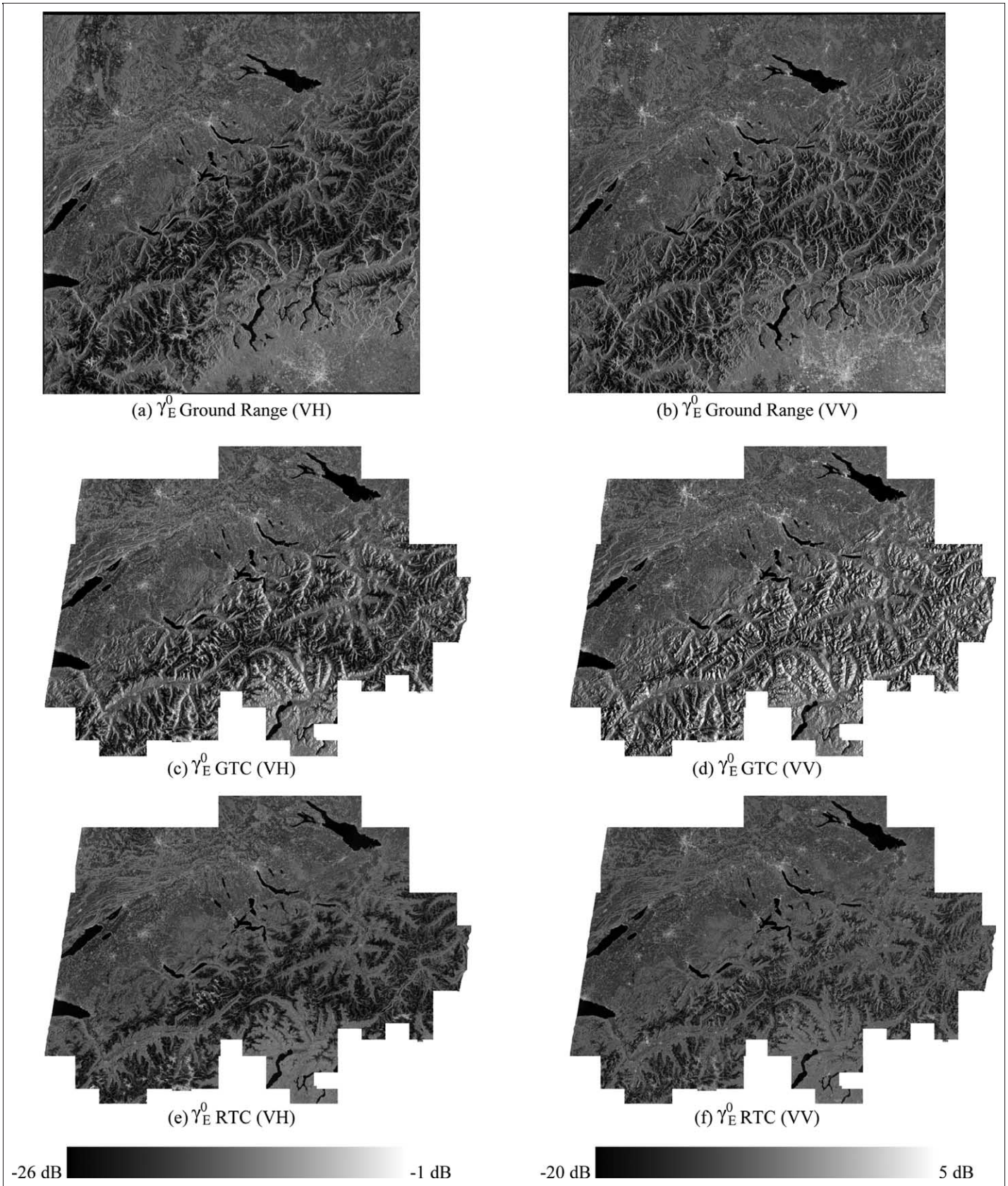

Figure 5. Radarsat-2 SCNB VH/VV, 27 April 2010, descending. DHM25 used for terrain geocoding and radiometric correction.

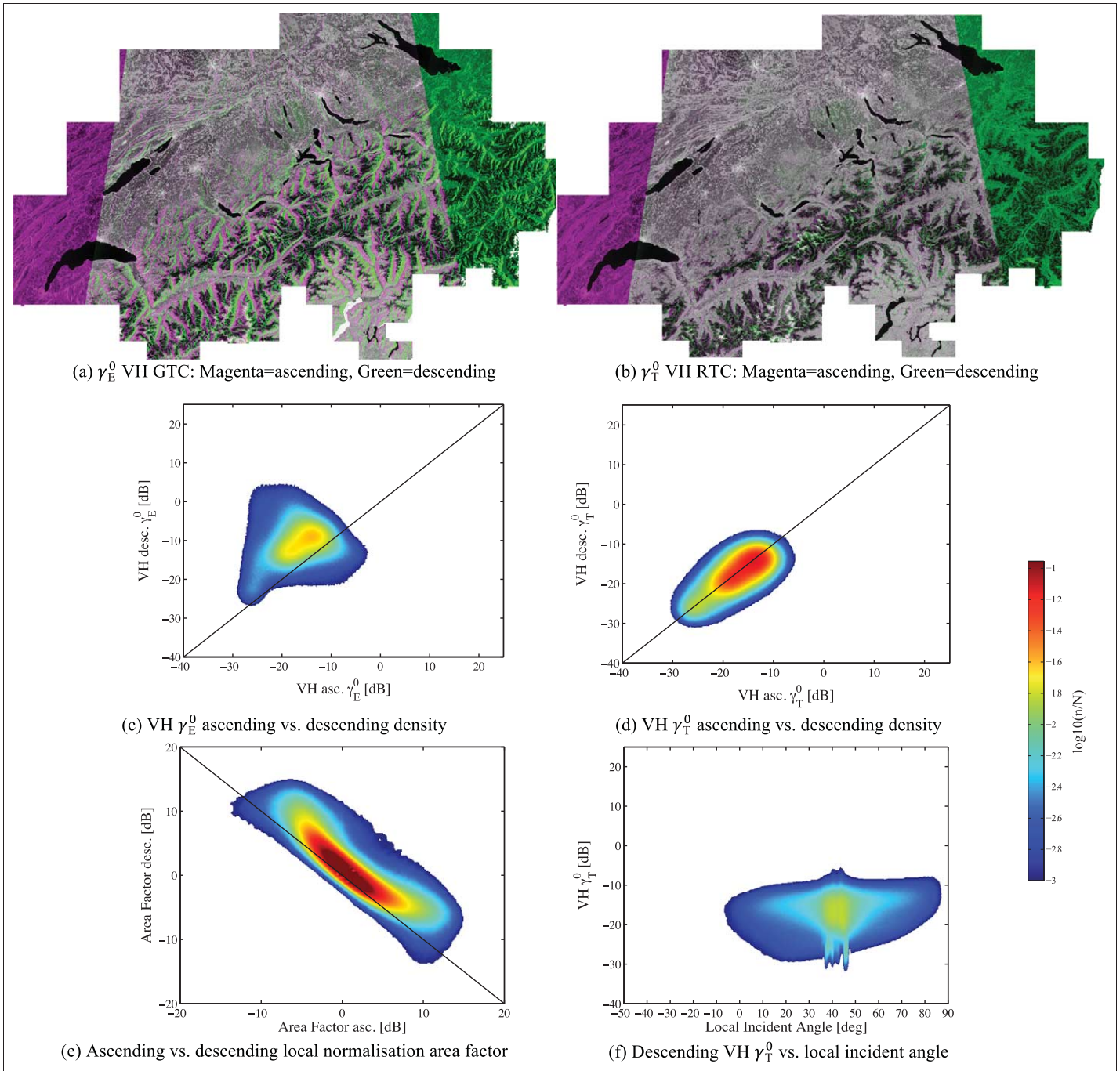

(a) γ^0_E VH GTC: Magenta=ascending, Green=descending

(b) γ^0_T VH RTC: Magenta=ascending, Green=descending

(c) VH γ^0_E ascending vs. descending density

(d) VH γ^0_T ascending vs. descending density

(e) Ascending vs. descending local normalisation area factor

(f) Descending VH γ^0_T vs. local incident angle

Figure 6. Radarsat-2 SCNB over Switzerland, ascending and descending comparisons. (a) γ^0_E VH GTC, (b) γ^0_T VH RTC, (c) VH γ^0_E A vs. D density, (d) VH γ^0_T A vs. D density, (e) A vs. D local normalisation area factor, (f) Descending VH γ^0_T vs. local incident angle.

factors of **Figure 6e** for the two configurations (ascending and descending). **Figure 6f** shows that terrain-flattened gamma nought is flat with respect to the local incident angle, a result consistent with that reported for more homogenous land cover in Small et al. (2010) and Small (2011). The dark areas near the 40° incident angle are caused by water bodies; the bright areas at the same angles are caused by settlements. Ensuring that backscatter retrievals become flat with respect to the incident angle requires that one not use the incident angle to directly determine the local reference area (e.g,. Kellndorfer et al., 1998). The reasons are described in Small et al. (2009b). One should instead use the more robust image simulation approach described in Small (2011).

Conclusions

The geolocation accuracies achieved without any refinement using tie points were reported for a set of two pairs

of R2 ultrafine and ScanSAR narrow products. Accurate tiepoint-free geolocation expedited treatment of terrain influences during backscatter retrieval, enabling multitrack backscatter comparisons, even ascending versus descending backscatter estimates in Alpine terrain. The narrow ScanSAR mode SCNB from R2 provided the closest approximant to the types of products that will become available from the Sentinel-1a and -1b satellites in the near future. The VH polarization appeared to be more sensitive to wet snow cover than the VV polarization. Terrain-flattened gamma nought products showed great potential for mapping dynamic wet snow cover in hilly and mountainous areas. They will improve comparability between multitrack backscatter estimates *within* the Sentinel-1 and Radarsat Constellation Missions (RCM), as well as *between* them. The terrain-flattened gamma nought backscatter standard would enable a theoretical near-worldwide 1 day revisit for the purposes of backscatter estimation given the availability of the planned Sentinel-1 and RCM satellites.

Acknowledgements

This work was supported in part by the European Space Agency under ESRIN/Contract No. 22501/09/I-EC. The Radarsat-2 data was provided by the Canadian Space Agency through its SOAR programme (project 1985). RADARSAT-2 Data and Products © MacDONALD, DETTWILER AND ASSOCIATES LTD. (2010) - All Rights Reserved. The digital height model DHM25 from swisstopo was used for terrain geocoding and radiometric corrections.

References

ESA, 2007. Information on ALOS PALSAR Products for ADEN Users. Frascati, Italy, *ALOS-GSEG-EOPG-TN-07-0001*. April 5, 2007.

Guindon, B., and Adair, M. 1992. Analytic formulation of spaceborne SAR image geocoding and "value-added" product generation procedures using digital elevation data, *Canadian Journal of Remote Sensing*, Vol. 18, pp. 2–12.

Kellndorfer, J.M., Pierce, M., Dobson, C., and Ulaby, F. 1998. Toward consistent regional-to-global-scale vegetation characterization using orbital SAR systems, *IEEE Transactions on Geoscience and Remote Sensing*, Vol. 36, No. 5, pp. 1396–1410. doi: 10.1109/36.718844.

MDA, Radarsat-2 Product Format Definition, RN-RP-51-2713, Issue 1/7, 14 March 2008, p. 5–40.

Meier, E., Frei, U., and Nüesch, D. 1993. Precise terrain corrected geocoded images, In: *SAR Geocoding: Data and Systems*, Schreier G. (Ed.), Herbert Wichmann Verlag, Germany, pp. 173–185.

Raney, K., Freeman, A., Hawkins, B., and Bamler, R. 1994. A plea for radar brightness, *Proceedings of International Geoscience and Remote Sensing Symposium IGARSS*, Pasadena, Calif., pp. 1090–1092. doi: 10.1109/IGARSS.1994.399352.

Rosich, B., and Meadows, P. 2004. Absolute calibration of ASAR Level 1 products generated with PF-ASAR, *ENVI-CLVL-EOPG-TN-03-0010*, Issue 1, Revision 5.

Schubert, A., Jehle, M., Small, D., and Meier, E. 2010. Influence of atmospheric path delay on the absolute geolocation accuracy of TerraSAR-X high-resolution products, *IEEE Transactions on Geoscience and Remote Sensing*, Vol. 48, No. 2, pp. 751–758. doi: 10.1109/TGRS.2009.2036252.

Small, D., Biegger, S., and Nüesch, D. 2000. Automated tiepoint retrieval through heteromorphic image simulation for spaceborne SAR sensors, *Proceedings of ESA ERS-ENVISAT Symposium*, Gothenburg, Sweden, 16–20 October 2000.

Small, D., Jehle, M., Meier, E., and Nüesch, D. 2004. Radiometric terrain correction incorporating local antenna gain, *Proceedings of the 5th European Conference on Synthetic Aperture Radar EUSAR*, Ulm, Germany, 25–27 May 2004.

Small, D., Rosich, B., Schubert, A., Meier, E., and Nüesch, D. 2004. Geometric validation of low and high-resolution ASAR imagery, *Proceedings of ENVISAT & ERS Symposium*, Salzburg, Austria, 6–10 September 2004, ESA SP-572, 9 p.

Small, D., Miranda, N., and Meier, E. 2009a. A revised radiometric normalization standard for SAR, *Proc. IGARSS*, Cape Town, South Africa, 13–17 July 2009, pp. 566–569. doi: 10.1109/IGARSS.2009.5417439.

Small, D., Miranda, N., and Meier, E. 2009b. Local incidence angle considered harmful, *Proceedings of CEOS SAR 2009 Cal/Val Workshop*, Pasadena, Calif, 17–19 November 2009. Available from http://www.ceos.org/images/WGCV/SAR/SESSION_2/2009-Session02-0150.pdf (accessed September 9, 2011)

Small, D., Miranda, N., Zuberbühler, L., Schubert, A., and Meier, E. 2010. Terrain-corrected gamma: improved thematic land-cover retrieval for SAR with robust radiometric terrain correction, *Proceedings of ESA Living Planet Symposium*, Bergen, Norway, 28 June – 2 July 2010, ESA SP-686, 8 p.

Small, D. 2011. Flattening gamma: radiometric terrain correction for SAR imagery, *IEEE Transactions on Geoscience and Remote Sensing*, Vol. 49, No. 8, pp. 3081–3093. doi: 10.1109/TGRS.2011.2120616.

swisstopo, 2005. DHM25: the digital height model of Switzerland – Product Information, 15 p.